Published in final edited form as:

Neuroimage. 2021 December 15; 245: 118658. doi:10.1016/j.neuroimage.2021.118658.

Investigating mechanisms of fast BOLD responses: the effects of stimulus intensity and of spatial heterogeneity of hemodynamics

Jingyuan E. Chen[a,b,*], **Gary H. Glover**[c], **Nina E. Fultz**[a,d], **Bruce R. Rosen**[a,b,e], **Jonathan R. Polimeni**[a,b,e], **Laura D. Lewis**[d]

[a]Athinoula A. Martinos Center for Biomedical Imaging, Massachusetts General Hospital, Boston, MA, USA

[b]Department of Radiology, Harvard Medical School, Boston, MA, USA

[c]Department of Radiology, Stanford University, Stanford, CA, USA

[d]Department of Biomedical Engineering, Boston University, Boston, MA, USA

[e]Harvard-Massachusetts Institute of Technology Division of Health Sciences and Technology, Cambridge, MA, USA

Abstract

Recent studies have demonstrated that fast fMRI can track neural activity well above the temporal limit predicted by the canonical hemodynamic response model. While these findings are promising, the biophysical mechanisms underlying these fast fMRI phenomena remain underexplored. In this study, we discuss two aspects of the hemodynamic response, complementary to several existing hypotheses, that can accommodate faster fMRI dynamics beyond those predicted by the canonical model. First, we demonstrate, using both visual and somatosensory paradigms, that the timing and shape of hemodynamic response functions (HRFs) vary across graded levels of stimulus intensity—with lower-intensity stimulation eliciting faster and narrower HRFs. Second, we show that as the spatial resolution of fMRI increases, voxel-wise HRFs begin to deviate from the canonical model, with a considerable portion of voxels exhibiting faster temporal dynamics than predicted by the canonical HRF. Collectively, both stimulus/task intensity and image resolution can affect the sensitivity of fMRI to fast brain activity, which may partly explain recent observations of fast fMRI signals. It is further noteworthy that, while the present investigations focus on fast neural responses, our findings suggest that a revised hemodynamic model may benefit the many fMRI studies using paradigms with wide ranges of contrast levels (e.g., resting or naturalistic conditions) or with modern, high-resolution MR acquisitions.

[*]Corresponding author: Jingyuan E. Chen, PhD., Athinoula A. Martinos Center for Biomedical Imaging, 149 Thirteenth St. Suite 2301, Charlestown, MA 02129 USA, Tel: +1 617 724 4546, Fax: +1 617 726 7422, jechen@mgh.harvard.edu.

Keywords

fast fMRI; hemodynamic response function; nonlinearity; task intensity; resting state; high spatial resolution

1 Introduction

Blood-oxygenation-level-dependent (BOLD) signals arise from an inherently sluggish hemodynamic process triggered by neural activity, posing an upper bound on the fastest neural fluctuations one can directly measure with fMRI. For instance, one of the widely-used canonical hemodynamic response functions (HRFs)—a two-Gamma-variate waveform routinely employed to model task-evoked fMRI responses provided by SPM (https://www.fil.ion.ucl.ac.uk/spm/)—predicts that the intensity of BOLD fluctuations should decay rapidly as a function of frequency and become minimal above 0.3 Hz. However, emerging evidence suggests that fMRI is capable of revealing neural activity occurring at faster time scales than this predicted limit. For instance, several studies have reported that resting-state functional connectivity, estimated from temporally synchronized BOLD fluctuations across distributed cortical areas, persists well beyond 0.3 Hz (Boubela et al., 2013; Chen and Glover, 2015; Gohel and Biswal, 2015; Lee et al., 2013; Lin et al., 2015; Trapp et al., 2018; Wang et al., 2018). Fast fMRI responses have also been identified in task-driven settings: significant BOLD fluctuations time-locked to high-frequency oscillatory stimuli have been characterized by a few groups, for instance, utilizing sensory paradigms in humans (up to 0.75 Hz (Fruhholz et al., 2020; Lewis et al., 2016)) and a gastric stimulus in rodents (0.8 Hz (Cao et al., 2019)). These empirical, fast fMRI observations therefore present an apparent contradiction to the canonical HRF model that is broadly used to infer or detect hemodynamic changes driven by neural dynamics.

To reconcile the apparent contradiction between fast fMRI observations and the sluggish nature of the conventional canonical HRF, several hypotheses have been proposed, including altered baseline cerebral blood flow (CBF) in response to sustained high-frequency stimuli (Lewis et al., 2016), intrinsic nonlinearity of neurovascular coupling (Buxton et al., 2004; Lewis et al., 2018; Miller et al., 2001; Vazquez and Noll, 1998), increased fractional contributions from non-T2/T2* mechanisms at higher frequencies (Chen and Glover, 2015), or possible artifacts in resting-state fMRI results arising from inappropriate data preprocessing (Chen et al., 2017). Despite these potential explanations for existing fast fMRI observations, a major open question is whether the canonical HRF itself—originally estimated using strong sensory stimuli and with conventional MR protocols (≥3 mm isotropic resolution plus extensive spatial smoothing)—should be revised for modern fMRI studies, in particular those that focus on fast fMRI phenomena. Rationales that motivate this argument are provided below.

The first rationale concerns emerging observations made with fast fMRI that show high-frequency signal fluctuations in the resting state. While it is still unclear why these fluctuations contain such high-frequency content, one possible perspective, embraced by several studies, is to view these intrinsic fluctuations as BOLD responses to varying levels

of internally-driven, potentially spontaneous neural events (Karahanoglu and Van De Ville, 2015; Liu and Duyn, 2013; Rangaprakash et al., 2018; Tagliazucchi et al., 2012; Wu et al., 2013). This perspective would suggest that the HRF for resting-state fluctuations may differ from the HRF for task-driven fMRI due to the potential nonlinearity of the BOLD response for short-duration and/or low-intensity stimuli. While multiple studies have investigated the effects of task intensity levels on fMRI responses, they focused mainly on the question of the nonlinearity of evoked signal amplitudes (Goodyear and Menon, 1998; Li et al., 2008; Liang et al., 2013; Liu et al., 2010; Marquardt et al., 2018; Mohamed et al., 2002; Vinke and Ling, 2020; Whittaker et al., 2016), and few studies have examined how the temporal features of HRFs might vary as a function of graded task intensities (Thompson et al., 2014; Yesilyurt et al., 2008). It may be possible that the resting-state BOLD signal can be explained with a variety of HRF timings whose temporal properties vary with the intensity of these neural events, perhaps with low-intensity fluctuations in neural activity triggering faster hemodynamic changes, thereby giving rise to the observed high-frequency BOLD fluctuations. How neural and hemodynamic processes contribute to task-intensity-dependent alterations in HRF speed has not yet been disambiguated, which is essential for understanding fast fMRI phenomena.

A second rationale for studying the frequency response of the HRF concerns the spatial resolution of fMRI protocols, which should also influence the temporal characteristics of the BOLD response. The experimentally derived canonical HRF and associated biophysical models were developed approximately two decades ago to model fMRI data collected with the conventional spatial resolutions utilized at that time (e.g., 3–4 mm isotropic voxel size, often followed by extensive smoothing) (Buxton et al., 1998; Friston et al., 2000; Mandeville et al., 1998). By contrast, modern fMRI studies (including several that focus on fast fMRI signals) employ a spatial resolution approaching millimeter scale or with more modest spatial smoothing (e.g., (Dumoulin et al., 2018; Lewis et al., 2016, 2018; Polimeni and Uludag, 2018; Yacoub and Wald, 2018)). As voxel size decreases, vascular anatomy governing the fMRI contrast mechanisms (e.g., vascular microstructure in tissue parenchyma vs. large draining vessels (Bianciardi et al., 2011; Kay et al., 2019; Lai et al., 1993; Uludag and Blinder, 2018); deep vs. superficial cortical depths (Havlicek and Uludag, 2020; Markuerkiaga et al., 2016; Siero et al., 2011; Tian et al., 2010)) becomes less homogenous, resulting in highly variable HRFs across voxels. While global-scale (brain-wide) or local-scale HRF variability has been extensively evaluated over the past two decades (e.g., (Gonzalez-Castillo et al., 2012; Handwerker et al., 2004; Lin et al., 2018; Rangaprakash et al., 2018; Puckett et al., 2014; Taylor et al., 2018)), its implication for fast fMRI dynamics has not yet been considered. Intuitively, if the canonical HRF only represents the group mean at relatively large voxel dimension, there must be certain voxels being more sensitive to faster brain dynamics (and of course certain voxels being less sensitive, e.g., parenchymal HRFs are measurably faster than superficial responses), therefore higher spatial resolution may reveal a subset of voxels that are more sensitive to high-frequency oscillations. This would thus suggest that the HRF itself can be faster than presumed by canonical models, even when using conventional task designs, and that fast fMRI dynamics in gray matter might simply be obscured by low-resolution imaging.

Motivated by these rationales, the goal of this study is to evaluate whether the timing and shape of the HRF can be modulated by task intensities and by the spatial resolution of fMRI, and could thus help explain the fast fMRI observations reported in existing literature. Accordingly, two lines of investigations are presented. In the first investigation, we employed two sets of sensory tasks (with simultaneous EEG signals also measured for the visual stimuli) to characterize how the HRF varied as a function of task intensity levels and to examine possible biophysical mechanisms underlying observed HRF alterations. In the second investigation, we collected both 3T and 7T high-resolution event-related task fMRI data to demonstrate spatially-varying features of HRFs and test whether responses that were faster than what is predicted by the canonical model could be detected. Although this study was motivated by an apparent disagreement between the canonical HRF and recent observations made with fast fMRI techniques, our findings also are relevant for the extensive body of fMRI studies that utilize paradigms with wide-ranging contrast levels (e.g., naturalistic stimuli) or with modern, high-resolution MR acquisitions.

2 Materials and methods

Two sets of experiments were carried out to investigate the modulation of task intensities and spatial resolution on HRFs. All experimental procedures were approved by the Massachusetts General Hospital or the Stanford Institutional Review Board, and all volunteers participated after providing written informed consent.

2.1 Modulation of task intensities on HRF shapes

The first set of experiments was aimed at: (1) examining how HRF timing varies as a function of stimulus intensities; and (2) elucidating possible neuronal and vascular contributions to task-intensity-dependent hemodynamic changes. The dependence of HRFs on stimulus intensities was assessed using two different sensory tasks (*2.1.1 Visual experiments* and *2.1.2 Somatosensory experiments*). We hypothesize that lower-intensity stimuli trigger HRFs that occur at faster temporal scales and can support elevated responses at higher frequencies.

2.1.1 Visual experiments

2.1.1.1 Experiments: 10 subjects (30±5 years old, 8 females) were enrolled for this experiment; their participation in different sessions are summarized in Table S1. Visual stimuli (radial checkerboards flickering at 7.5 Hz) were implemented with Matlab-based psychtoolbox (http://psychtoolbox.org) (Kleiner M, 2007) and presented on a rear-projection screen viewed through a mirror fixed in front of the subjects' eyes. An event-related paradigm with inter-trial intervals randomly jittered between 5–20 s was employed to characterize HRFs associated with two distinct luminance levels (high contrast (9 trials per scan): 30% vs. low contrast (14 trials per scan): 1.8%). Given the nonlinearity in sensory perception, a baseline luminance level (1%) instead of a neutral-gray background (0%) was displayed in order to maximize the separability of neuronal and hemodynamic responses characterized at the two employed contrast levels. Two different trial durations (6 s vs. 1 s) were examined for both luminance levels in order to assess the additional modulation imposed by HRF nonlinearities, i.e., how the contrast modulation differed between long and

short trial durations (Vazquez and Noll, 1998). Timing of an exemplar task scan is shown in Fig. 1A. Each subject underwent 4–7 6-s-trial scans during the 1st study visit, and a subset of six subjects returned for a 2nd study visit to perform additional 6–10 1-s-trial scans (Table S1).

2.1.1.2 Acquisition: Simultaneous EEG/MR data were collected on a 3T Siemens Prisma scanner (Siemens Healthineers, Erlangen, Germany) with a vendor-supplied 64-channel head-and-neck coil. *High-resolution anatomical images:* T_1-weighted multi-echo magnetization-prepared rapid gradient-echo (MPRAGE) images (van der Kouwe et al., 2008) (1.0 mm isotropic spatial resolution, TR = 2530 ms, TE = 1.69, 3.55, 5.41, 7.27 ms, flip angle = 7°, FOV = 256×256×176 mm, and acceleration factor $R = 2$) were acquired for anatomical reference. *Functional images:* A standard inter-leaved multiple-slice EPI (nominal voxel size = 1.2×1.2×1.5 mm^3, TR = 857 ms, TE = 34 ms, flip angle = 53°, FOV = 130×113 mm, 10 slices with no gap covering the calcarine sulcus, phase-encode partial Fourier factor = 7/8, echo spacing = 0.76 ms, bandwidth = 1522 Hz/pixel, and acceleration factor $R = 1$) was used to track task-evoked functional changes in the BOLD signal. To achieve broader brain coverage for better across-scan registration, a reference EPI scan with extended slice coverage (containing 36 slices and 6 time frames, distortion-matched and position-matched to the fMRI protocol) was additionally collected at the end of each task scan.

Concurrent EEG data were collected for the 6-s-trial scans, and were recorded with MR-compatible 256-channel geodesic nets and a NA410 amplifier (Electrical Geodesics, Inc.). Data were sampled at 1,000 Hz and referenced to the Cz electrode. The EEG system clock was synchronized with the MRI scanner's 10-MHz master synthesizer to align data sampling with the gradient artifact; and a TR trigger was fed into the EEG system at the beginning of each volume acquisition to facilitate denoising of gradient artifacts via template subtraction. To remove ballistocardiogram artifacts, a reference-layer based approach (Luo et al., 2014) was employed. MR scanner coldheads were switched off during all EEG sessions to further mitigate scanner noise contributions. Given the relatively low signal-to-noise ratio (SNR) of each EEG trial response compared to fMRI signals, we appended 2–3 additional short EEG-only task scans to increase the total number of EEG trials, with MR acquisition off and reduced inter-trial intervals (jittered between 5–8 s, 16 high-/10 low-contrast trials per scan), prior to the concurrent EEG/fMRI scans for each subject.

2.1.1.3 Occipital fMRI responses elicited by graded visual stimuli: After motion and slice timing correction using AFNI (https://afni.nimh.nih.gov), functional images of different task scans were co-registered using Boundary-Based Registration (Greve and Fischl, 2009) as implemented in the FreeSurfer (https://surfer.nmr.mgh.harvard.edu) command *bbregister*, with the between-scan rigid transformation matrix estimated from the reference EPI data (with larger brain coverage) collected at the end of each task scan to the T_1-weighted anatomical reference image. Task-active voxels were identified by general linear model (GLM) analysis, with task-evoked responses to lower- and higher-contrast stimuli separately modeled by convolving the SPM canonical HRF and its temporal derivative with the corresponding timing paradigm of either luminance level (i.e., 4 task

regressors in total). An F-test was carried out to evaluate the significance of detectable task activation (total variance explained by the 4 task regressors) in each voxel. After localizing task-active voxels, each voxel's fMRI time series was linearly interpolated to a 0.5 s temporal grid; and fMRI responses for different luminance levels and trial durations were derived using the finite impulse response (FIR) deconvolution approach (Glover, 1999), implemented through AFNI. For each luminance level/duration, fMRI responses of separate task scans were integrated using a fixed-effect model.

2.1.1.4 Contrast-dependent hemodynamic changes as a function of cortical depths: Given the distinct vascular anatomy of the pial surface and parenchyma, we further examined if this contrast modulation of HRF shapes differed across cortical depths. Surface-based cortical depth estimation was performed using the T_1-weighted anatomical reference (MPRAGE); normalized cortical depth ('0%': white/gray matter boundary; '100%' pial) of each EPI voxel was computed according to its centroid coordinate (Polimeni et al., 2010; Polimeni et al., 2018). Task-active voxels (F-score > 10) were separated into five groups based on their normalized cortical depths (D1:0–40%, D2:40–80%, D3:80–120%, D4:120–160%, D5:160–200%, where depths > 100% denote locations above the cortex); mean fMRI responses within each cortical depth were computed for further comparisons. To assess the sensitivity of findings to the chosen statistical threshold, F-score value was varied from 5 to 15.

2.1.1.5 Electrophysiological responses time-locked to 6-s task trials: For concurrent EEG/fMRI scans, gradient artifacts in the EEG recordings caused by the MR scanning environment were removed by template subtraction implemented in the Fieldtrip toolbox (http://www.fieldtriptoolbox.org). For both EEG-only and EEG/fMRI scans, electrodes were re-referenced to the common average, computed separately for electrodes contacting the head and sham electrodes insulated from the scalp. Channels on the cheeks were excluded from computing the common average. Ballistocardiogram artifacts were estimated from sham electrodes and projected out of signals from true EEG electrodes using a time-varying regression approach (Fultz et al., 2019). We specifically focused on two EEG signatures that have been separately linked with the primary peak (Bianciardi et al., 2009; Lewis et al., 2016) and post-stimulus undershoot (PSU) (Mullinger et al., 2017; Wilson et al., 2019) of HRFs previously: the steady-state visually-evoked potentials (SSVEPs, 7.5 Hz) and the occipital alpha wave (8–12 Hz). The spectra of occipital electrodes were inspected and the electrode demonstrating the strongest SSVEP or alpha activity (manifested as sharp peaks in the standard frequency band) was manually picked for each EEG signature respectively, i.e., the chosen electrodes for SSVEP and alpha activity can be different. Hilbert transforms of band-passed EEG signals (SSVEP: 7.4–7.6 Hz and alpha wave: 8–12 Hz) were computed and averaged across all 6-s task trials (from both EEG-only and EEG/fMRI scans) to reflect the strength of SSVEPs and alpha activity time-locked to the stimulation. To calculate SSVEP amplitude changes over time, the slope of the SSVEP amplitude during the stimulus-on period was fitted by linear regression separately in the high-contrast and low-contrast conditions. Confidence interval (CI) values for the change in SSVEP amplitude were estimated using bootstrapping (resampling 1000 times over subjects with replacement, and

each bootstrap sample had the same number of subjects as the original dataset) (Lewis et al., 2018).

2.1.1.6 Testing whether scalp EEG signatures can predict task-contrast-dependent HRF patterns: After characterizing the strengths of SSVEP and alpha wave time-locked to the 6-s visual stimuli, we next simulated whether task-contrast-dependent alterations in these neural dynamics, if they exist, could account for characterized fMRI changes across luminance levels. Given the lack of direct evidence linking SSVEP and alpha wave activity, their respective impacts were evaluated independently via two models described as follows. *Model* I ('Balloon Model'): we first took a forward biophysical modeling approach to simulate cascading BOLD changes in response to specific neural activity (SSVEP or alpha activity) and gauged whether the resultant BOLD dynamics agreed with the empirical fMRI observations. This was implemented through previously described biophysical models (Buxton et al., 2004; Buxton et al., 1998). Briefly, we assumed a linear neurovascular relationship, invoking a Gamma-variate function to link neural activity (i.e., envelopes of SSVEP and alpha wave amplitudes) and cerebral blood flow (CBF), and used the balloon model for subsequent flow-volume transformations (Buxton et al., 2004). *Model II* ('Deconvolution Model'): to minimize the dependence on prior assumptions and avoid any bias related to our selection of balloon model parameter values, we additionally performed a simple, alternative analysis that linearly deconvolved the impulse HRF linking EEG recordings and fMRI observations (with envelopes of SSVEP and alpha activity as inputs and empirical fMRI responses as outputs). The resulting HRFs for different luminance levels (i.e., $HRF_{1.8\%}$ and $HRF_{30\%}$) were anticipated to only reflect hemodynamic components. Detailed descriptions and parameters of both models are presented in Supplementary Material SM1.

2.1.2 Somatosensory experiments—To examine the generalizability of the measured HRF alterations across cortical regions, we additionally evaluated the modulation of task contrast levels on somatosensory HRFs through a vibrotactile stimulus.

2.1.2.1 Experiments: Eleven subjects (35±14 years old, 6 females, all right-handed) were enrolled for this experiment. Each subject participated in four task sessions, with each session consisting of 17 task trials (number of trials = 7/5/5 for low/medium/high intensities respectively, 6-s on and 25-s off per trial). Throughout the experiment, the subject's right hand rested on a sponge with two vibrotactile piezoelectric stimulators (manufactured by the Dancer Design, http://dancerdesign.co.uk) taped to the index and middle fingers. During the *'on'* period, one of the two stimulators was randomly activated every 0.25 s to alleviate sensory adaptation; the activated stimulator stayed on for 0.25 s and oscillated at 100 Hz. Subjects were instructed to look at a fixed cross at the center of the screen and refrain from attending to the vibrotactile stimulation to mitigate potential confounds caused by attention.

2.1.2.2 Acquisition: MR images were collected on a 3T GE scanner (GE Healthcare, Waukesha, WI, USA). *High-resolution anatomical images:* T_2-weighted fast spin-echo structural images (voxel size = 0.86×0.86×4 mm^3, TR = 3000 ms, TE = 68 ms, echo train length = 12, FOV = 220×220×128 mm) were acquired for anatomical reference.

Functional images: two different acquisition protocols were used for BOLD-weighted functional acquisitions: *Acq. I* (sub 01–08, on a GE Signa Discovery 750 scanner with a vendor-supplied 8-channel head coil): a gradient-echo spiral-in/out pulse sequence (Glover and Law, 2001) was used for T_2* weighted functional imaging (voxel size = 3.44×3.44×4 mm^3, TR = 700 ms, TE = 30 ms, flip angle = 53°, FOV = 220×220 mm, 10 slices with no gap); *Acq. II* (sub 09–11, on a GE Premier scanner with a vendor-supplied 48-channel head coil): a simultaneous multi-slice (SMS) EPI sequence with blipped controlled aliasing in parallel imaging (CAIPI) sequence (Setsompop et al., 2012) was used for T_2* weighted functional imaging (voxel size = 2.39×2.39×4 mm^3, TR = 700 ms, TE = 30 ms, flip angle = 53°, FOV = 220×220 mm, 30 slices with no gap, SMS acceleration factor = 3).

2.1.2.3 Somatosensory fMRI responses elicited by graded vibrotactile stimuli: After motion and slice timing correction using AFNI and across-scan registration using FSL, a GLM analysis was carried out to identify task-active voxels (akin to section 2.1.1.3, with 6 task regressors in total for three different contrast levels). Each voxel's time course was further resampled to a 0.5 s temporal grid. Given the long inter-trial intervals (25 s), voxel-wise fMRI responses triggered by different vibrating intensities were derived by trial-based temporal averaging. For each subject and each task contrast level, task-evoked fMRI responses across different scans were integrated using a fixed-effect model.

2.2 Effects of fMRI spatial resolution on HRF speed

Apart from task intensities, a second factor considered in this study hypothesized to influence measured HRF speed is the fMRI spatial resolution. As voxel size is reduced, BOLD signals become less homogenous across voxels and are likely to increasingly depart from the canonical model. We therefore hypothesized that high-spatial-resolution acquisitions will uncover a higher degree of spatial heterogeneity in the HRF, including responses that are both faster and slower than the canonical HRF timing. These faster responses seen in a subset of voxels would exhibit an increased sensitivity to higher-frequency fluctuations than what would be predicted by the canonical HRF. In this new set of experiments, we focused on the inter-voxel variability of HRFs in visual cortex in response to brief visual stimuli and measured using high-resolution MR protocols (approaching 1 mm isotropic resolution and below), and evaluated how the heterogeneity of voxel-wise HRF features vary as a function of image resolution.

2.2.1 Experiments—Ten subjects (27±4 years old, 6 females) were enrolled for this experiment. Each subject underwent multiple event-related visual task scans (with the stimulus set-up identical to that described in section 2.1.1.1), during which the subjects viewed flickering checkerboards with stimulus timing patterns following a pseudo-random M-sequence paradigm (Buracas and Boynton, 2002). The base interval of the M-sequence was 0.5 s, and the total duration of each task scan was 255 s. Five subjects were scanned on a 3T scanner (5–6 scans per subject) and five subjects were scanned on a 7T scanner (7–13 scans per subject).

2.2.2 Acquisition—3T acquisition: MR images were collected on a 3T Siemens Prisma scanner with a vendor-supplied 64-channel head-and-neck coil. *High-resolution anatomical*

images: T_1-weighted MPRAGE images (nominal 1 mm isotropic voxel size, TR = 2530 ms, TE = 1.69, 3.55, 5.41, 7.27 ms, flip angle = 7°, FOV = 256×256×176 mm, and acceleration factor $R = 2$) were acquired for anatomical reference. *Functional images:* A standard inter-leaved multiple-slice EPI (nominal voxel size = 1.2×1.2×1.5 mm, TR = 780 ms, TE = 34 ms, flip angle = 53°, FOV = 130×113 mm, 9 slices with no gap, phase partial Fourier factor = 7/8, echo spacing = 0.76 ms, bandwidth = 1522 Hz/pixel) was used to measure the BOLD response. 7T acquisition: MR images were collected on a 7T Siemens MAGNETOM whole-body scanner equipped with SC72 body gradients and a custom-built 32-channel head coil (Keil, 2010). *High-resolution anatomical images:* High-resolution T_1-weighted MPRAGE images (nominal 0.75 mm isotropic voxel size, TR = 2530 ms, TE = 1.76, 3.70 ms, flip angle = 7°, FOV = 240×240×168 mm, and acceleration factor $R = 2$) were acquired for anatomical reference. *Functional images:* A standard single-shot inter-leaved multiple-slice EPI (nominal 0.8 mm isotropic voxel size, TR = 1010 ms, TE = 28 ms, flip angle = 70°, FOV = 192×192 mm, 15 slices with no gap, acceleration factor $R = 4$, phase partial Fourier factor = 7/8, nominal echo spacing = 1 ms, bandwidth =1185 Hz/pixel) was used to map brain functional changes. A reference EPI scan with extended slice coverage (31 slices, 2 time frames, distortion-matched and position-matched to the fMRI protocol) was collected during each session to facilitate across-scan registration.

2.2.3 Voxel-wise HRFs—

After motion and slice timing correction using AFNI, 3T functional images of different scans were coregistered directly using Robust Registration (Reuter et al., 2010) as implemented in the *mri_robust_register* command in FreeSurfer; 7T functional images of different scans were coregistered indirectly through the rigid transformation matrices estimated from reference images (with larger brain coverage) appended at the end of each task scan and T_1-weighted anatomical images using *bbregister*. A GLM-based F-test was carried out to identify voxels exhibiting significant task effects (modeled by convolving the SPM canonical HRF with the M-sequence paradigm); the temporal derivative of the task response was also modelled and included in GLM. The time course of each voxel was linearly interpolated to the 0.5 s temporal grid to match the base resolution of M-sequence; then the hemodynamic responses triggered by the 0.5-s-long visual trial was deconvolved for each voxel using FIR. Voxel-wise HRFs of different task scans were integrated using a fixed-effect model for each subject.

2.2.4 Influence of spatial resolution on the heterogeneity of HRF speed—

Several metrics were computed to quantify the heterogeneous shapes and spectral properties of HRFs in task-active areas: ‘TTP’: time to peak; ‘FWHM’: full-width at half-maximum; and ‘$A_{0.2}/A_{0.1}$’: the ratio of frequency response (i.e., the Fourier transform of HRF time course) at 0.2 Hz and 0.1 Hz. Voxel-wise HRFs were fitted by a set of HRF bases (described in Supplementary Material SM2) prior to deriving these summary metrics. To assess if higher spatial resolutions enhance detection of faster hemodynamics (capturing HRFs with earlier TTPs, narrower FWHMs and elevated $A_{0.2}/A_{0.1}$), we spatially smoothed the functional images with an isotropic 3D Gaussian kernel (FWHM = 2, 4, and 8 mm), and re-evaluated voxel-wise HRFs and the distribution of various HRF metrics.

3 Results

3.1 Effect of task intensities on evoked HRF speed and electrophysiological dynamics

We observed distinct timings in fMRI responses elicited by visual stimuli of different contrast levels (Fig. 1B, C). Compared to the high-contrast stimuli (30% luminance level), fMRI block-responses evoked by the low-contrast stimuli (1.8% luminance level) exhibited faster temporal features, including earlier TTPs (by 0.47±0.42 s across subjects, paired *t* test $p = 1.0\times1e^{-3}$), reduced FWHMs (by 0.56±0.47 s across subjects, paired *t* test $p = 6.2\times1e^{-4}$), and slightly diminished post-stimulus undershoots (PSUs). These contrast-dependent differences in HRF timing also appeared to be duration-dependent in the cohort of six subjects participating in both '6-s' and '1-s' scans: fMRI responses evoked by the 1-s weaker stimuli only peaked 0.09±0.40 s earlier (paired *t* test $p = 0.59$) and had 0.43±0.27 s narrower FWHMs (paired *t* test $p = 5.6\times1e^{-3}$) than those evoked by the stronger stimuli, suggesting that task intensity might affect BOLD responses in a task-duration-dependent manner.

Timing of cortical-depth-dependent fMRI responses and their dependence on the task contrast level are shown in Fig. 2. Limited by the voxel size, we could not resolve laminar-specific signals and information was blurred across depths. For both luminance levels, responses measured at the pial surface and above lagged those measured at deeper cortical depths, agreeing with previous reports (Lewis et al., 2018; Markuerkiaga et al., 2016; Siero et al., 2011; Tian et al., 2010) (Fig. 2A). The contrast-dependent changes in HRF speed (i.e., reduced TTP and FWHM at the lower contrast level) were consistent across cortical depths (Fig. 2B). Paired *t* test of TTPs between task intensities yields: D1: $p = 4.1\times1e^{-3}$, D2: $p = 6.2\times1e^{-3}$, D3: $p = 1.6\times1e^{-3}$, D4: $p = 0.13$, D5: $p = 0.10$; and paired *t* test of FWHMs between task intensities yields: D1: $p = 9.9\times1e^{-3}$, D2: $p = 5.6\times1e^{-3}$, D3: $p = 0.041$, D4: $p = 0.026$, D5: $p = 1.8\times1e^{-3}$. These results suggest that the contrast dependence of HRF timing is not impacted by the distinct levels of the vascular hierarchy sampled at various cortical depths.

Both neural and hemodynamic effects could contribute to the observed differences in fMRI responses across conditions. To investigate possible neural contributions to the faster hemodynamic changes to lower-contrast stimuli, we analyzed the EEG data concurrently recorded during the fMRI sessions. The measured EEG responses were consistent with a higher level of neural activity in the higher-contrast condition—the during-stimulus percent magnitude increase of SSVEP was ~1-fold larger, and the percent magnitude decrease of occipital alpha activity was ~50% stronger for the higher-contrast condition than the lower-contrast condition (Fig. 3A). Contrast-dependent changes were also observed in both the SSVEP and alpha envelope patterns (Fig. 3A). SSVEP power in response to the higher-contrast stimuli demonstrated a more evident increase throughout the stimulation period than the lower-contrast stimuli (*t* test on SSVEP slopes, $p < 10^{-5}$). Alpha power dropped relative to baseline during the stimulation period for both contrasts and exhibited a slightly more pronounced post-stimulus overshoot for the higher-contrast stimuli—the 95% confidence interval (CI) of the ratio of higher- vs. lower-contrast alpha intensity level was [1.34 1.79] during stimulus (mean across 0–6 s) and [2.17 7.89] following the stimulus

(mean across 7–9 s). However, despite the qualitative differences in the EEG responses to the two stimulus conditions, the EEG signatures only explained a modest fraction of the differences in the measured BOLD responses associated with the luminance level. While our forward modeling of based on either SSVEP or alpha activity (*Model I* 'Balloon Model') predicted a simulated BOLD response with slightly faster TTP and a diminished post-stimulus undershoot of the lower-contrast fMRI responses, neither electrophysiological measure could account for the narrower FWHM seen in the measured fMRI data in response to the lower-contrast task (Fig. 3 'simulated $BOLD_{6s}$' vs. 'measured $BOLD_{6s}$'). Not surprisingly, the impulse HRF, after deconvolving the neural responses, still demonstrated contrast-dependent patterns that partly recapitulate the features of the BOLD responses prior to deconvolution (*Model II* 'Deconvolution Model'): $HRF_{1.8\%}$ exhibited a faster TTP and a much narrower FWHM than $HRF_{30\%}$ (Fig. 3 'deconvolved *HRF*'). Collectively, these observations suggest that, in addition to SSVEP and alpha oscillations investigated here, observed HRF timing difference also arise from alternative neural or vascular mechanisms.

To test the generalizability of contrast-induced HRF differences outside of visual cortex, we also characterized somatosensory fMRI responses evoked by vibrotactile stimuli (Fig. 4A). The summary metrics of fMRI responses associate with graded stimuli levels are shown in Fig. 4B. Compared to the strongest stimuli ('*High*'), fMRI responses evoked by the weaker stimuli demonstrated faster TTPs ('*Medium*': 0.71±0.71 s faster across subjects, paired t test $p = 0.038$; '*Low*': 1.63±0.42 s faster across subjects, paired t test $p = 5.2\times10^{-5}$); and narrower FWHMs ('*Medium*': 0.06±0.74 s narrower across subjects, paired t test $p = 0.84$; '*Low*': 1.48±1.06 s narrower across subjects, paired t test $p = 0.011$). We analyzed TTP and FWHM results from seven subjects, because the remaining four subjects did not exhibit a significant task-dependent HRF (three subjects failed to demonstrate significant activation for each stimulus and one subject did not exhibit an evoked response with varying magnitude across task intensities, i.e., the requirement of a task-driven HRF for characterizing contrast-dependent alterations in timing was not met). However, for completeness, task-evoked fMRI results from all 11 subjects are shown in Supplementary Material SM3. Consistent with the pattern observed in visual cortex, the low-intensity vibrating stimuli caused faster TTPs and narrower FWHMs in postcentral gyrus, providing further evidence that the influence of task intensity level ought to be considered when modeling fMRI dynamics, at least in sensory cortex and perhaps beyond. We thus conclude that data from distinct sensory modalities showed a consistent increase in HRF speed in response to low-intensity stimuli.

3.2 Modulation of image spatial resolution on the heterogeneity of HRF speed

Our second set of experiments were aimed at evaluating whether fast HRFs were preferentially observed with high-resolution functional imaging due to reduced signal blurring across heterogeneous tissue vasculature. We investigated the distribution of HRF speed across voxels using brief visual stimuli and at higher spatial resolutions than the data reported above. Figure 5 summarizes the distributions of TTPs, FWHMs, and frequency-specific power ratios (between high- and low-frequency fMRI responses) of HRFs across task-active voxels averaged across all subjects. For both 3T and 7T results, we observed remarkable variability of temporal features across adjacent voxels, and identified a

considerable portion of voxels with the potential to accommodate faster responses than the canonical model—the fastest HRFs exhibited ~1.5 s earlier TTP, ~1.8 s narrower FWHMs, and >1-fold higher $A_{0.2}/A_{0.1}$ than the canonical HRF (TTP = 5 s, FWHM = 5.3 s, and $A_{0.2}/A_{0.1}$ = 0.17). Deviations of these parameters from the canonical model became more modest as the image spatial resolution was reduced (3D Gaussian smoothing kernel size FWHM = 2/4/8 vs. 0 mm).

4 Discussion

4.1 General findings

In this study, by evaluating sensory HRFs associated with different task contrasts and spatial resolutions, we demonstrated that both lower stimulus intensity levels and higher spatial resolutions can result in faster BOLD responses. There are two major observations of our study. (1) Stimuli with smaller intensity levels can lead to faster TTPs, narrower FWHMs and diminished PSUs in the resulting HRFs. This contrast modulation of HRFs is more pronounced for long-duration stimuli, and is consistent across cortical depths. In addition, concurrently measured SSVEPs and alpha wave activity also demonstrate task-intensity-dependent neural changes that can predict certain features of altered HRF timing at lower task intensities (earlier TTPs and less prominent PSUs). (2) By applying high-spatial-resolution MR acquisitions, we further demonstrate that a considerable portion of voxel-wise HRFs have the potential to reflect faster hemodynamic changes than the canonical model. In the following, we will first discuss possible biophysical mechanisms underlying these empirical observations, then consider potential implications that our results may hold for future fMRI studies, and finally highlight a few technical limitations that warrant further investigations in the future.

4.2 Neural and vascular contributions to stimulus-intensity-dependent HRF patterns

Both SSVEP and alpha wave activity investigated here exhibited clear differences between lower and higher luminance contrast levels, supporting distinct neural responses as one candidate mechanism driving contrast-dependent HRF differences. It has been previously demonstrated that the SSVEP can be modulated by attention, and exhibits higher amplitudes when the subject attends to the stimuli (Hillyard et al., 1997; Itthipuripat et al., 2019; Kim et al., 2007; Morgan et al., 1996). Therefore, the distinct SSVEP patterns we observed across the two luminance intensities—i.e., with a steady increasing amplitude observed during the stimulus period for the higher-intensity stimulus but not for the lower-intensity stimulus—might be due to sustained attention throughout the higher-contrast stimulation period, in contrast to faster adaptation for the lower-intensity trials. Likewise, contrast-dependent attentional load may also account for the differences in alpha desynchronization during the stimulus (Klimesch, 2012; Pfurtscheller and Lopes da Silva, 1999). Because the power of both EEG signatures peaked earlier for the lower-contrast stimuli, the simulated HRF exhibited a slightly faster TTP than that elicited by the higher-contrast stimuli, agreeing with the experimental results. In addition to the distinct neural responses observed during the stimulus, a less pronounced post-stimulus overshoot in alpha power was also seen in the lower-contrast stimuli. Alpha activity has been postulated to reflect the level of inhibitory neural process, with stronger alpha synchronization corresponding to reduced

cortical excitability (Jensen and Mazaheri, 2010; Klimesch et al., 2007; Pfurtscheller et al., 1994; Pfurtscheller et al., 1996). Stronger alpha power has been hypothesized to reflect stronger inhibitory neural activity post stimulus, and was reported to correlate with more pronounced HRF PSU (Mullinger et al., 2017; Wilson et al., 2019), consistent with the patterns seen in our data. While our forward modeling results based on SSVEP and alpha wave signatures, together with this consistency with previous reports, can explain some aspects of the contrast-dependent HRF features (TTPs and PSUs), a comprehensive picture of neurophysiological underpinnings of our observations remains to be determined. For instance, in addition to the EEG signatures examined here, gamma-band local field potentials also correlate with stimulus-driven hemodynamic changes (Logothetis et al., 2001); a necessary follow-up investigation will be to query if the modulation of task intensities on elicited gamma-band activity, through scalp EEG with enhanced signal quality or invasive electrode recordings, can provide better predictions of observed changes in HRF timing.

Complementary to these neural mechanisms, potential vascular changes may also cause intensity-dependent HRF timing differences, including the narrower FWHM seen for the lower-intensity stimuli, which was not explained by the EEG measurements. A few related possibilities may contribute to this effect. First, this intensity-dependent HRF nonlinearity may arise partly from the nonlinear transformation of CBF responses to BOLD responses (Buxton et al., 2004; Miller et al., 2001). To qualitatively predict how HRF features vary as a function of the CBF amplitudes, we performed a simple simulation based on the balloon model (as described in Supplementary Material SM4). A stronger CBF response (i.e., a higher peak amplitude) produced a slightly wider FWHM and an accentuated PSU that aligns with our empirical observations (Fig. S4). A second possibility lies in the potential modulation of task intensities on the quantitative relationships between different contributors to BOLD signals (Chen and Pike, 2009; Liang et al., 2013; Whittaker et al., 2016). For instance, if the steady-state flow-volume coupling ratio increases with the stimulus intensity (Chen and Pike, 2009), a stronger stimulus may elicit a larger PSU given the dependence of PSU on blood volume changes. Moreover, if the weaker stimulus results in reduced arterial dilation and reduced CBF, which in turn results in reduced pressure being delivered to the draining venules, this may cause decreased passive venous compliance as compared to the stronger stimulus (in a manner analogous to distinct vascular dynamics triggered by brief vs. prolonged stimuli (Drew et al., 2011)), which may also produce a narrower FWHM and diminished PSU. Realistic biophysical models that account for these dynamics may provide insight on these vascular effects (Pfannmoeller et al., 2020). Collectively, even if stimulus-driven neural activity and associated biochemical signaling are consistent across task contrasts, these intensity-dependent vascular effects may also produce the observed HRF timing differences across task intensities.

4.3 Possible biophysical mechanisms underlying faster hemodynamic changes relative to the canonical HRF

Amplified across-voxel variability of HRFs at high spatial resolutions (Fig. 5) can result from multiple biophysical factors beyond simply the spatially-varying contrast-to-noise ratios. For instance, hemodynamic delays across cortical depths have been demonstrated

by several studies (Havlicek and Uludag, 2020; Lewis et al., 2018; Markuerkiaga et al., 2016; Siero et al., 2011; Tian et al., 2010). Smaller voxel sizes can ameliorate across-depth signal blurring and resolve deep cortical voxels with faster temporal dynamics (Lewis et al., 2018). Apart from this well-characterized, systematic change in HRF timing with cortical depth, in general, voxel-by-voxel differences in vascular anatomy becomes more evident as the voxel size decreases—factors such as fractional venous contributions (Bause et al., 2020; Kay et al., 2019; Moerel et al., 2018; Uludag and Blinder, 2018), variable vessel orientation relative to the main magnetic field (Baez-Yanez et al., 2017; Gagnon et al., 2015; Viessmann et al., 2019), all of which are themselves dependent on the specific fMRI acquisition parameters, will play a more dominant role in determining the observed hemodynamic patterns. Consequently, the canonical HRF model may no longer be adequate to capture the diversity of HRF timings observable at high spatial resolution. As a simple illustration of how the spatial heterogeneity of HRF timing is associated with local vascular anatomy, Fig. 6 shows an additional dataset consisting of high-resolution time-of-flight data acquired along with high-resolution BOLD fMRI responses to visual stimuli acquired in human visual cortex to characterize hemodynamic responses in voxels containing small vessels (see Supplementary Material SM5 for acquisition and task details). As shown in Fig. 6, the HRFs of voxels containing large vessels (identified as punctate image features with brighter contrast in the angiography data (Fig. 6A) caused by larger inflow effects) and voxels dominated by smaller vessels (identified as darker contrast in the angiography data) clearly diverge (Fig. 6B)—the former still resemble canonical HRF patterns, whereas the latter (‘*Scaled*’, highlighted in green) demonstrate transient features that cannot be fully explained by the classical hemodynamic model. Smaller voxel sizes can thus better portray the variability of HRF timing and speed, and can isolate faster hemodynamic changes that would otherwise be blurred with larger voxel sizes.

In addition to resolving the subset of voxels presenting faster temporal dynamics, fast fMRI signals also benefit from higher spatial resolution in the sense of mitigating intra-voxel phase cancellation, which is more problematic for higher-frequency than lower-frequency fluctuations due to shorter duration per cycle. For instance, for a temporal lag of 1 s (e.g., parenchymal vs. superficial HRF), the phase cancellation between early and late HRFs could occur for 0.5 Hz brain functional oscillations (Fig. 7, ‘0.1 Hz’ vs. ‘0.5 Hz’ oscillations). A similar empirical observation has been made by previous work showing that vascular lags between early and late V1 hemodynamic responses elicited by 0.75 Hz oscillatory flickering checkerboard patterns could be up to half a task cycle, such that dramatic BOLD signal cancellation would occur, as shown in our simulations, if the spatial resolution were not sufficiently high (Lewis et al., 2016).

4.4 Implications for fMRI studies

A first implication of our findings is that a single HRF (e.g., the canonical HRF) may not suffice to summarize the transformation from neural activity to fMRI observations under scenarios when a wide range of stimulus/task intensities are used. This observation is particularly relevant for fMRI studies using resting-state or naturalistic task conditions, as opposed to the large, slow changes induced by conventional block-design paradigms. The neurovascular coupling patterns subserving spontaneous resting-state fluctuations remain

controversial: on one hand, our results demonstrate faster hemodynamics associated with lower stimulus intensities, and, if the resting-state can be viewed as low-intensity neuronal fluctuations, our findings may help explain recent observations of high-frequency resting-state BOLD observations (e.g., Chen and Glover, 2015; Gohel and Biswal, 2015; Lee et al., 2013; Trapp et al., 2018); on the other hand, using blind- or EEG-informed deconvolution of resting-state BOLD data, a few groups have estimated that the HRF for resting-state BOLD may be at a similar or even slower temporal scale than the canonical HRF (de Munck et al., 2007; Tagliazucchi et al., 2012; Wu et al., 2013), which to some extent mirrors the conventional notion that spontaneous activities are dominated by ultra-slow fluctuations below 0.1 Hz. Possibly, these complementary observations could be reconciled by acknowledging the co-existence of multiple HRF patterns (varying timing and shapes) at resting state, corresponding to internally-driven or spontaneous neural events occurring at different temporal frequencies and different amplitudes or intensities. Likewise, the neural activity driven by naturalistic stimuli (e.g., movie watching or auditory tones) may also exhibit a range of different temporal frequencies and different amplitudes given that natural stimuli are known to contain sensory and cognitive stimuli at diverse scales and intensities. In parallel to conventional investigations that focus on brain-wide connectivity patterns modulated by naturalistic stimuli, emerging reports on fast fMRI observations have also inspired efforts to uncover rich information linked with fast, brief neural dynamics (Gao, 2015), in which case, incorporation of contrast-dependent hemodynamic models can be beneficial.

A second, and direct, implication of our findings is that moving toward higher spatial resolutions may enhance the likelihood of capturing faster brain dynamics that cannot be detected in lower spatial resolutions, provided that the temporal sampling rate is above the Nyquist rate to resolve the frequency of interest. While there is always a trade-off between specificity and detectability, smaller voxel sizes may not necessarily result in a dramatic loss in SNR due to the reduced partial volume effects that can reduce noise contamination of the gray matter BOLD signal (Blazejewska et al., 2019; Polimeni et al., 2018), as evidenced by the higher percent signal changes of task-active voxels (up to 10% in Fig. 1B) than those reported in studies with conventional MR protocols (1–2%). Furthermore, low SNR can be compensated by signal averaging—either using anatomically-informed smoothing that averages fMRI signals in anatomical regions expected to have similar hemodynamics (e.g., within cortical depths) or, as an extension of this concept, using “hemodynamically-informed” smoothing not across spatially contiguous voxels but rather those in coherent response phases.

4.5 Potential limitation and future directions

This study would benefit from further animal experiments in various aspects. First, while both visual and vibrotactile stimuli had successfully evoked graded changes in HRFs, only a modest distinction across task contrasts was observed, i.e., the lowest-intensity stimuli still evoked an observable response in the form of considerable deviation from the baseline (e.g., 4% signal change by the 1.8% luminance contrast in the visual experiment, shown in Fig. 1B). It is challenging in practice, due to limited dynamic range and SNR, to induce a wide range of fMRI responses, including very large and very small responses—that are

still detectable—needed for fully characterizing the hypothesized differences in timing. Animal experiments could enable sufficient repetitions of task trials such that responses evoked by very subtle contrast levels can be detected. Second, it is challenging to eliminate the confounds of task-coupled attention in awake humans, which however, can potentially be circumvented by examining involuntary responses through anesthetic administration or optogenetic manipulations (Boyden et al., 2005), although these approaches present their own confounds in both hemodynamics and neural regime. Third, it remains unclear which EEG signatures are the most effective for assessing the net excitation-inhibition balance that drives the local energy demand and the associated hemodynamics that generate the BOLD response. In this sense, while both SSVEP and alpha power have previously been demonstrated to correlate with hemodynamic changes (Bianciardi et al., 2009; Goldman et al., 2002; Lewis et al., 2016; Mullinger et al., 2017), their exact roles as direct or indirect causes of specific hemodynamic responses are still unclear, therefore it is difficult to interpret their contributions to task-contrast-dependent HRF observations. Moreover, while previous studies have shown that SSVEP originates from the primary visual area (di Russo et al., 2007; Müller et al., 1997), errors caused by volume conduction may still exist in our data due to the lack of accurate EEG source localization. With direct access to excitatory and inhibitory synaptic activity and vascular physiology through invasive electrophysiological and optical measurements, rodent studies would open a promising avenue to better understand contrast- dependent neuronal, and neurovascular aspects in future studies.

In this study, we only briefly discussed how different HRF timings can lead to different sensitivities to detecting fast brain dynamics. A natural extension in future investigations will be to establish a comprehensive model that incorporates measures of fine-scale vascular anatomy and hemodynamics with fMRI physics, and characterize the specific stimulus configuration most favorable to probe high-frequency neural dynamics with fMRI, which should hold practical value in guiding future studies. In addition, as our study used supra-millimetre voxel sizes, substantial blurring of differences across cortical layers is expected in our data, and future studies at high spatial resolution could further elucidate these dynamics. Finally, while both visual and somatosensory HRFs demonstrated consistent dependence on the task intensity levels, the employment of different acquisition protocols at two independent institutes has posed a challenge in assessing the inter-region variability of characterized HRF nonlinearity, which can be resolved by invoking consistent acquisitions in future investigations.

In conclusion, our findings demonstrate that both reduced task contrast and enhanced spatial resolution can lead to faster HRF timing, which may increase the sensitivity of fMRI to detect fast brain dynamics. These insights will be helpful in designing experiments that can exploit these fast hemodynamics, and additionally, contribute to the growing body of evidence provoking the community to reconsider the biophysical limits of fMRI and the potential of fast fMRI. While investigations herein were initially motivated by an interest in elucidating fast fMRI dynamics, they also hold implications for modeling BOLD dynamics in emerging fMRI studies that utilize wide dynamic range stimuli such as naturalistic paradigms and modern MR acquisitions with increased spatial resolution.

Supplementary Material

Refer to Web version on PubMed Central for supplementary material.

Acknowledgements

The authors acknowledge Drs. Sam Ling, Joshua Foster, Kawin Setsompop, Avery Berman and Joerg Pfannmoeller for valuable discussions regarding the present results; Mr. Ned Ohringer for assistance with data acquisition; and three anonymous reviewers for their constructive comments, which have substantially improved the quality of the manuscript. This work was supported in part by the National Institute of Biomedical Imaging and Bioengineering at the National Institutes of Health (grant numbers P41-EB015891, P41-EB015896, R01-EB019437), by the *BRAIN Initiative* (National Institute of Mental Health at the National Institute of Health: grant numbers R01-MH111438, R01-MH111419), by the National Institute of Neurological Disorders and Stroke (grant number K99-NS118120), by the National Institute of Mental Health at the National Institute of Health (grant number R00-MH111748), and by the MGH/HST Athinoula A. Martinos Center for Biomedical Imaging; and was made possible by the resources provided by NIH Shared Instrumentation grants S10-OD010759, S10-RR023043 and S10-RR019371.

References

Baez-Yanez MG, Ehses P, Mirkes C, Tsai PS, Kleinfeld D, Scheffler K, 2017. The impact of vessel size, orientation and intravascular contribution on the neurovascular fingerprint of BOLD bSSFP fMRI. Neuroimage 163, 13–23. [PubMed: 28890417]

Bause J, Polimeni JR, Stelzer J, In MH, Ehses P, Kraemer-Fernandez P, Aghaeifar A, Lacosse E, Pohmann R, Scheffler K, 2020. Impact of prospective motion correction, distortion correction methods and large vein bias on the spatial accuracy of cortical laminar fMRI at 9.4 Tesla. Neuroimage 208, 116434. [PubMed: 31812715]

Bianciardi M, Bianchi L, Garreffa G, Abbafati M, Di Russo F, Marciani MG, Macaluso E, 2009. Single-epoch analysis of interleaved evoked potentials and fMRI responses during steady-state visual stimulation. Clin Neurophysiol 120, 738–747. [PubMed: 19250866]

Bianciardi M, Fukunaga M, van Gelderen P, de Zwart JA, Duyn JH, 2011. Negative BOLD-fMRI signals in large cerebral veins. J Cereb Blood Flow Metab 31, 401–412. [PubMed: 20859295]

Blazejewska AI, Fischl B, Wald LL, Polimeni JR, 2019. Intracortical smoothing of small-voxel fMRI data can provide increased detection power without spatial resolution losses compared to conventional large-voxel fMRI data. Neuroimage 189, 601–614. [PubMed: 30690157]

Boubela RN, Kalcher K, Huf W, Kronnerwetter C, Filzmoser P, Moser E, 2013. Beyond Noise: Using Temporal ICA to Extract Meaningful Information from High-Frequency fMRI Signal Fluctuations during Rest. Front Hum Neurosci 7, 168. [PubMed: 23641208]

Boyden ES, Zhang F, Bamberg E, Nagel G, Deisseroth K, 2005. Millisecond-timescale, genetically targeted optical control of neural activity. Nat Neurosci 8, 1263–1268. [PubMed: 16116447]

Buracas GT, Boynton GM, 2002. Efficient design of event-related fMRI experiments using M-sequences. Neuroimage 16, 801–813. [PubMed: 12169264]

Buxton RB, Uludag K, Dubowitz DJ, Liu TT, 2004. Modeling the hemodynamic response to brain activation. Neuroimage 23 Suppl 1, S220–233. [PubMed: 15501093]

Buxton RB, Wong EC, Frank LR, 1998. Dynamics of blood flow and oxygenation changes during brain activation: the balloon model. Magn Reson Med 39, 855–864. [PubMed: 9621908]

Cao J, Lu KH, Oleson ST, Phillips RJ, Jaffey D, Hendren CL, Powley TL, Liu Z, 2019. Gastric stimulation drives fast BOLD responses of neural origin. Neuroimage 197, 200–211. [PubMed: 31029867]

Chen JE, Glover GH, 2015. BOLD fractional contribution to resting-state functional connectivity above 0.1 Hz. Neuroimage 107, 207–218. [PubMed: 25497686]

Chen JE, Jahanian H, Glover GH, 2017. Nuisance Regression of High-Frequency Functional Magnetic Resonance Imaging Data: Denoising Can Be Noisy. Brain Connect 7, 13–24. [PubMed: 27875902]

Chen JJ, Pike GB, 2009. BOLD-specific cerebral blood volume and blood flow changes during neuronal activation in humans. NMR Biomed 22, 1054–1062. [PubMed: 19598180]

de Munck JC, Goncalves SI, Huijboom L, Kuijer JP, Pouwels PJ, Heethaar RM, Lopes da Silva FH, 2007. The hemodynamic response of the alpha rhythm: an EEG/fMRI study. Neuroimage 35, 1142–1151. [PubMed: 17336548]

di Russo F, Pitzalis S, Aprile T, Spitoni G, Patria F, Stella A, Spinelli D, Hillyard SA, 2007. Spatiotemporal analysis of the cortical sources of the steady-state visual evoked potential. Human Brain Mapping 28.

Drew PJ, Shih AY, Kleinfeld D, 2011. Fluctuating and sensory-induced vasodynamics in rodent cortex extend arteriole capacity. Proc Natl Acad Sci U S A 108, 8473–8478. [PubMed: 21536897]

Dumoulin SO, Fracasso A, van der Zwaag W, Siero JCW, Petridou N, 2018. Ultra-high field MRI: Advancing systems neuroscience towards mesoscopic human brain function. NeuroImage 168, 345–357. [PubMed: 28093360]

Friston KJ, Mechelli A, Turner R, Price CJ, 2000. Nonlinear responses in fMRI: the Balloon model, Volterra kernels, and other hemodynamics. Neuroimage 12, 466–477. [PubMed: 10988040]

Fruhholz S, Trost W, Grandjean D, Belin P, 2020. Neural oscillations in human auditory cortex revealed by fast fMRI during auditory perception. Neuroimage 207, 116401. [PubMed: 31783116]

Fultz NE, Bonmassar G, Setsompop K, Stickgold RA, Rosen BR, Polimeni JR, Lewis LD, 2019. Coupled electrophysiological, hemodynamic, and cerebrospinal fluid oscillations in human sleep. Science 366, 628–631. [PubMed: 31672896]

Gagnon L, Sakadzic S, Lesage F, Musacchia JJ, Lefebvre J, Fang Q, Yucel MA, Evans KC, Mandeville ET, Cohen-Adad J, Polimeni JR, Yaseen MA, Lo EH, Greve DN, Buxton RB, Dale AM, Devor A, Boas DA, 2015. Quantifying the microvascular origin of BOLD-fMRI from first principles with two-photon microscopy and an oxygen-sensitive nanoprobe. J Neurosci 35, 3663–3675. [PubMed: 25716864]

Gao JS, 2015. fMRI Visualization and Methods. University of California, Berkeley.

Glover GH, 1999. Deconvolution of impulse response in event-related BOLD fMRI. Neuroimage 9, 416–429. [PubMed: 10191170]

Glover GH, Law CS, 2001. Spiral-in/out BOLD fMRI for increased SNR and reduced susceptibility artifacts. Magn Reson Med 46, 515–522. [PubMed: 11550244]

Gohel SR, Biswal BB, 2015. Functional integration between brain regions at rest occurs in multiple-frequency bands. Brain Connect 5, 23–34. [PubMed: 24702246]

Goldman RI, Stern JM, Engel J Jr., Cohen MS, 2002. Simultaneous EEG and fMRI of the alpha rhythm. Neuroreport 13, 2487–2492. [PubMed: 12499854]

Gonzalez-Castillo J, Saad ZS, Handwerker DA, Inati SJ, Brenowitz N, Bandettini PA, 2012. Whole-brain, time-locked activation with simple tasks revealed using massive averaging and model-free analysis. Proc Natl Acad Sci U S A 109, 5487–5492. [PubMed: 22431587]

Goodyear BG, Menon RS, 1998. Effect of luminance contrast on BOLD fMRI response in human primary visual areas. J Neurophysiol 79, 2204–2207. [PubMed: 9535979]

Greve DN, Fischl B, 2009. Accurate and robust brain image alignment using boundary-based registration. Neuroimage 48, 63–72. [PubMed: 19573611]

Handwerker DA, Ollinger JM, D'Esposito M, 2004. Variation of BOLD hemodynamic responses across subjects and brain regions and their effects on statistical analyses. Neuroimage 21, 1639–1651. [PubMed: 15050587]

Havlicek M Uludag K, 2020. A dynamical model of the laminar BOLD response. Neuroimage 204, 116209. [PubMed: 31546051]

Hillyard SA, Hinrichs H, Tempelmann C, Morgan ST, Hansen JC, Scheich H, Heinze HJ, 1997. Combining steady-state visual evoked potentials and f MRI to localize brain activity during selective attention. Hum Brain Mapp 5, 287–292. [PubMed: 20408230]

Itthipuripat S, Sprague TC, Serences JT, 2019. Functional MRI and EEG Index Complementary Attentional Modulations. J Neurosci 39, 6162–6179. [PubMed: 31127004]

Jensen O, Mazaheri A, 2010. Shaping functional architecture by oscillatory alpha activity: gating by inhibition. Front Hum Neurosci 4, 186. [PubMed: 21119777]

Karahanoglu FI, Van De Ville D, 2015. Transient brain activity disentangles fMRI resting-state dynamics in terms of spatially and temporally overlapping networks. Nat Commun 6, 7751. [PubMed: 26178017]

Kay K, Jamison KW, Vizioli L, Zhang R, Margalit E, Ugurbil K, 2019. A critical assessment of data quality and venous effects in sub-millimeter fMRI. Neuroimage 189, 847–869. [PubMed: 30731246]

Keil B, Triantafyllou C, Hamm M, Wald LL, 2010. Design optimization of a 32-channel head coil at 7T. Proc Intl Soc Mag Reson Med. 18, 1493.

Kim YJ, Grabowecky M, Paller KA, Muthu K, Suzuki S, 2007. Attention induces synchronization-based response gain in steady-state visual evoked potentials. Nat Neurosci 10, 117–125. [PubMed: 17173045]

Kleiner M, B. D, Pelli D, 2007. What's new in Psychtoolbox-3? Perception 36, 1.

Klimesch W, 2012. alpha-band oscillations, attention, and controlled access to stored information. Trends Cogn Sci 16, 606–617. [PubMed: 23141428]

Klimesch W, Sauseng P, Hanslmayr S, 2007. EEG alpha oscillations: the inhibition-timing hypothesis. Brain Res Rev 53, 63–88. [PubMed: 16887192]

Lai S, Hopkins AL, Haacke EM, Li D, Wasserman BA, Buckley P, Friedman L, Meltzer H, Hedera P, Friedland R, 1993. Identification of vascular structures as a major source of signal contrast in high resolution 2D and 3D functional activation imaging of the motor cortex at 1.5T: preliminary results. Magn Reson Med 30, 387–392. [PubMed: 8412613]

Lee HL, Zahneisen B, Hugger T, LeVan P, Hennig J, 2013. Tracking dynamic resting-state networks at higher frequencies using MR-encephalography. Neuroimage 65, 216–222. [PubMed: 23069810]

Lewis LD, Setsompop K, Rosen BR, Polimeni JR, 2016. Fast fMRI can detect oscillatory neural activity in humans. Proc Natl Acad Sci U S A 113, E6679–E6685. [PubMed: 27729529]

Lewis LD, Setsompop K, Rosen BR, Polimeni JR, 2018. Stimulus-dependent hemodynamic response timing across the human subcortical-cortical visual pathway identified through high spatiotemporal resolution 7T fMRI. Neuroimage 181, 279–291. [PubMed: 29935223]

Li X, Lu ZL, Tjan BS, Dosher BA, Chu W, 2008. Blood oxygenation level-dependent contrast response functions identify mechanisms of covert attention in early visual areas. Proc Natl Acad Sci U S A 105, 6202–6207. [PubMed: 18413602]

Liang CL, Ances BM, Perthen JE, Moradi F, Liau J, Buracas GT, Hopkins SR, Buxton RB, 2013. Luminance contrast of a visual stimulus modulates the BOLD response more than the cerebral blood flow response in the human brain. Neuroimage 64, 104–111. [PubMed: 22963855]

Lin FH, Chu YH, Hsu YC, Lin JF, Tsai KW, Tsai SY, Kuo WJ, 2015. Significant feed-forward connectivity revealed by high frequency components of BOLD fMRI signals. Neuroimage 121, 69–77. [PubMed: 26208871]

Lin FH, Polimeni JR, Lin JL, Tsai KW, Chu YH, Wu PY, Li YT, Hsu YC, Tsai SY, Kuo WJ, 2018. Relative latency and temporal variability of hemodynamic responses at the human primary visual cortex. Neuroimage 164, 194–201. [PubMed: 28119135]

Liu X, Duyn JH, 2013. Time-varying functional network information extracted from brief instances of spontaneous brain activity. Proc Natl Acad Sci U S A 110, 4392–4397. [PubMed: 23440216]

Liu Z, Rios C, Zhang N, Yang L, Chen W, He B, 2010. Linear and nonlinear relationships between visual stimuli, EEG and BOLD fMRI signals. Neuroimage 50, 1054–1066. [PubMed: 20079854]

Logothetis NK, Pauls J, Augath M, Trinath T and Oeltermann A, 2001. Neurophysiological investigation of the basis of the fMRI signal. Nature 412, 150–157. [PubMed: 11449264]

Luo Q, Huang X, Glover GH, 2014. Ballistocardiogram artifact removal with a reference layer and standard EEG cap. J Neurosci Methods 233, 137–149. [PubMed: 24960423]

Mandeville JB, Marota JJ, Kosofsky BE, Keltner JR, Weissleder R, Rosen BR, Weisskoff RM, 1998. Dynamic functional imaging of relative cerebral blood volume during rat forepaw stimulation. Magn Reson Med 39, 615–624. [PubMed: 9543424]

Markuerkiaga I, Barth M, Norris DG, 2016. A cortical vascular model for examining the specificity of the laminar BOLD signal. Neuroimage 132, 491–498. [PubMed: 26952195]

Marquardt I, Schneider M, Gulban OF, Ivanov D, Uludag K, 2018. Cortical depth profiles of luminance contrast responses in human V1 and V2 using 7 T fMRI. Hum Brain Mapp 39, 2812–2827. [PubMed: 29575494]

Miller KL, Luh WM, Liu TT, Martinez A, Obata T, Wong EC, Frank LR, Buxton RB, 2001. Nonlinear temporal dynamics of the cerebral blood flow response. Hum Brain Mapp 13, 1–12. [PubMed: 11284042]

Moerel M, De Martino F, Kemper VG, Schmitter S, Vu AT, Ugurbil K, Formisano E, Yacoub E, 2018. Sensitivity and specificity considerations for fMRI encoding, decoding, and mapping of auditory cortex at ultra-high field. Neuroimage 164, 18–31. [PubMed: 28373123]

Mohamed FB, Pinus AB, Faro SH, Patel D, Tracy JI, 2002. BOLD fMRI of the visual cortex: quantitative responses measured with a graded stimulus at 1.5 Tesla. J Magn Reson Imaging 16, 128–136. [PubMed: 12203759]

Morgan ST, Hansen JC, Hillyard SA, 1996. Selective attention to stimulus location modulates the steady-state visual evoked potential. Proc Natl Acad Sci U S A 93, 4770–4774. [PubMed: 8643478]

Müller MM, Teder W, Hillyard SA, 1997. Magnetoencephalographic recording of steady-state visual evoked cortical activity. Brain Topography 9.

Mullinger KJ, Cherukara MT, Buxton RB, Francis ST, Mayhew SD, 2017. Post-stimulus fMRI and EEG responses: Evidence for a neuronal origin hypothesised to be inhibitory. Neuroimage 157, 388–399. [PubMed: 28610902]

Pfannmoeller JP, G. L, Berman AL, Polimeni JR, 2020. The role of rapid capillary resistance decreases in the BOLD response assessed through simulations in a realistic vascular network. Proc Intl Soc Mag Reson Med. 28, 1101.

Pfurtscheller G, Lopes da Silva FH, 1999. Event-related EEG/MEG synchronization and desynchronization: basic principles. Clin Neurophysiol 110, 1842–1857. [PubMed: 10576479]

Pfurtscheller G, Neuper C, Mohl W, 1994. Event-related desynchronization (ERD) during visual processing. Int J Psychophysiol 16, 147–153. [PubMed: 8089033]

Pfurtscheller G, Stancak A Jr., Neuper C, 1996. Event-related synchronization (ERS) in the alpha band--an electrophysiological correlate of cortical idling: a review. Int J Psychophysiol 24, 39–46. [PubMed: 8978434]

Polimeni JR, Fischl B, Greve DN, Wald LL, 2010. Laminar analysis of 7T BOLD using an imposed spatial activation pattern in human V1. Neuroimage 52, 1334–1346. [PubMed: 20460157]

Polimeni JR, Renvall V, Zaretskaya N, Fischl B, 2018. Analysis strategies for high-resolution UHF-fMRI data. Neuroimage 168, 296–320. [PubMed: 28461062]

Polimeni JR, Uludag K, 2018. Neuroimaging with ultra-high field MRI: Present and future. Neuroimage 168,1–6. [PubMed: 29410013]

Puckett AM, Mathis JR, DeYoe EA, 2014. An investigation of positive and inverted hemodynamic response functions across multiple visual areas. Hum Brain Mapp 35, 5550–5564. [PubMed: 25044672]

Rangaprakash D, Wu GR, Marinazzo D, Hu X, Deshpande G, 2018. Hemodynamic response function (HRF) variability confounds resting - state fMRI functional connectivity. Magnetic resonance in medicine, 80, 1697–1713. [PubMed: 29656446]

Reuter M, Rosas HD, Fischl B, 2010. Highly accurate inverse consistent registration: a robust approach. Neuroimage 53, 1181–1196. [PubMed: 20637289]

Setsompop K, Gagoski BA, Polimeni JR, Witzel T, Wedeen VJ, Wald LL, 2012. Blipped-controlled aliasing in parallel imaging for simultaneous multislice echo planar imaging with reduced g-factor penalty. Magn Reson Med 67, 1210–1224. [PubMed: 21858868]

Siero JC, Petridou N, Hoogduin H, Luijten PR, Ramsey NF, 2011. Cortical depth-dependent temporal dynamics of the BOLD response in the human brain. J Cereb Blood Flow Metab 31, 1999–2008. [PubMed: 21505479]

Tagliazucchi E, Balenzuela P, Fraiman D, Chialvo DR, 2012. Criticality in large-scale brain FMRI dynamics unveiled by a novel point process analysis. Front Physiol 3, 15. [PubMed: 22347863]

Taylor AJ, Kim JH, Ress D, 2018. Characterization of the hemodynamic response function across the majority of human cerebral cortex. Neuroimage 173, 322–331. [PubMed: 29501554]

Thompson SK, Engel SA, Olman CA, 2014. Larger neural responses produce BOLD signals that begin earlier in time. Front Neurosci 8, 159. [PubMed: 24971051]

Tian P, Teng IC, May LD, Kurz R, Lu K, Scadeng M, Hillman EM, De Crespigny AJ, D'Arceuil HE, Mandeville JB, Marota JJ, Rosen BR, Liu TT, Boas DA, Buxton RB, Dale AM, Devor A, 2010. Cortical depth-specific microvascular dilation underlies laminar differences in blood oxygenation level-dependent functional MRI signal. Proc Natl Acad Sci U S A 107, 15246–15251. [PubMed: 20696904]

Trapp C, Vakamudi K, Posse S, 2018. On the detection of high frequency correlations in resting state fMRI. Neuroimage 164, 202–213. [PubMed: 28163143]

Uludag K, Blinder P, 2018. Linking brain vascular physiology to hemodynamic response in ultra-high field MRI. Neuroimage 168, 279–295. [PubMed: 28254456]

van der Kouwe AJW, Benner T, Salat DH, Fischl B, 2008. Brain morphometry with multiecho MPRAGE. Neuroimage 40, 559–569. [PubMed: 18242102]

Vazquez AL, Noll DC, 1998. Nonlinear aspects of the BOLD response in functional MRI. Neuroimage 7, 108–118. [PubMed: 9558643]

Viessmann O, Scheffler K, Bianciardi M, Wald LL, Polimeni JR, 2019. Dependence of resting-state fMRI fluctuation amplitudes on cerebral cortical orientation relative to the direction of B0 and anatomical axes. Neuroimage 196, 337–350. [PubMed: 31002965]

Vinke LN, Ling S, 2020. Luminance potentiates human visuocortical responses. J Neurophysiol 123, 473–483. [PubMed: 31825699]

Wang Y, Zhu L, Zou Q, Cui Q, Liao W, Duan X, Biswal B, Chen H, 2018. Frequency dependent hub role of the dorsal and ventral right anterior insula. Neuroimage 165, 112–117. [PubMed: 28986206]

Whittaker JR, Driver ID, Bright MG, Murphy K, 2016. The absolute CBF response to activation is preserved during elevated perfusion: Implications for neurovascular coupling measures. Neuroimage 125, 198–207. [PubMed: 26477657]

Wilson R, Mullinger KJ, Francis ST, Mayhew SD, 2019. The relationship between negative BOLD responses and ERS and ERD of alpha/beta oscillations in visual and motor cortex. Neuroimage 199, 635–650. [PubMed: 31189075]

Wu GR, Liao W, Stramaglia S, Ding JR, Chen H, Marinazzo D, 2013. A blind deconvolution approach to recover effective connectivity brain networks from resting state fMRI data. Med Image Anal 17, 365–374. [PubMed: 23422254]

Yacoub E, Wald LL, 2018. Pushing the spatio-temporal limits of MRI and fMRI. Neuroimage 164, 1–3. [PubMed: 29254519]

Yesilyurt B, Ugurbil K, Uludag K, 2008. Dynamics and nonlinearities of the BOLD response at very short stimulus durations. Magn Reson Imaging 26, 853–862. [PubMed: 18479876]

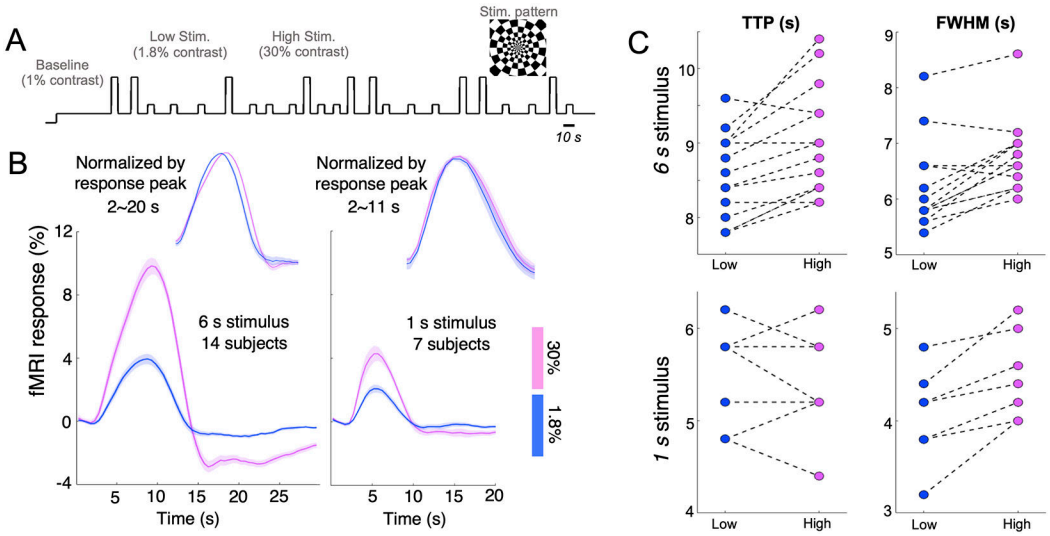

Figure 1.

(A) Timing of a single visual task session (an exemplar 6-s-trial case). (B) Evoked fMRI responses across task contrasts and trial durations, averaged across 100 voxels demonstrating the strongest task activation (mean and standard errors across subjects). Sub-periods of fMRI responses (2–20 s for the '6 s stimulus' and 2–11 s for the '1 s stimulus') are normalized by peak response intensities and displayed atop the raw responses for comparison. Qualitative changes associated with the 6-s lower-contrast HRF (faster TTPs, Narrower FWHMs and diminished PSUs) remained when the number of task-active voxels was increased to 500, 1,000 and 2,000. (C) Summary of TTPs and FWHMs of fMRI responses evoked by different task contrasts and trial durations (each dashed line connects the results from the same subject).

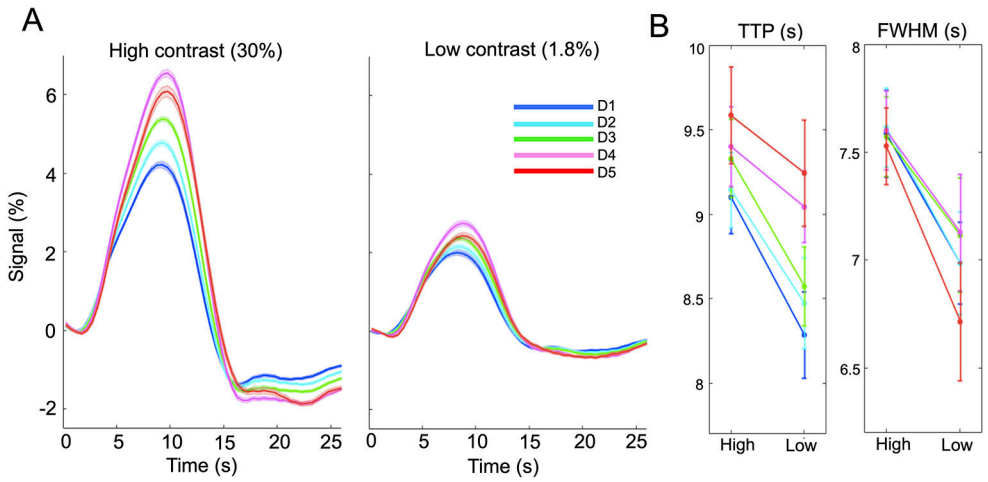

Figure 2.

Contrast-dependent fMRI patterns across cortical depths (6-s trial case, task-active voxels with F-score > 10). (A) Cortical-depth-dependent HRFs evoked by lower and higher luminance levels (mean and standard errors across subjects), with depths D1–D5 defined in 2.1.1.4; (B) Reduced TTPs and FWHMs of lower-contrast HRFs. Contrast-dependent TTP and FWHM alterations remained if the F-score threshold was varied from 5 to 15, except that in a few subjects' results, the percent signal change of the above-pial HRF ('red') became smaller than those in deeper depths when we lowered the F-score threshold.

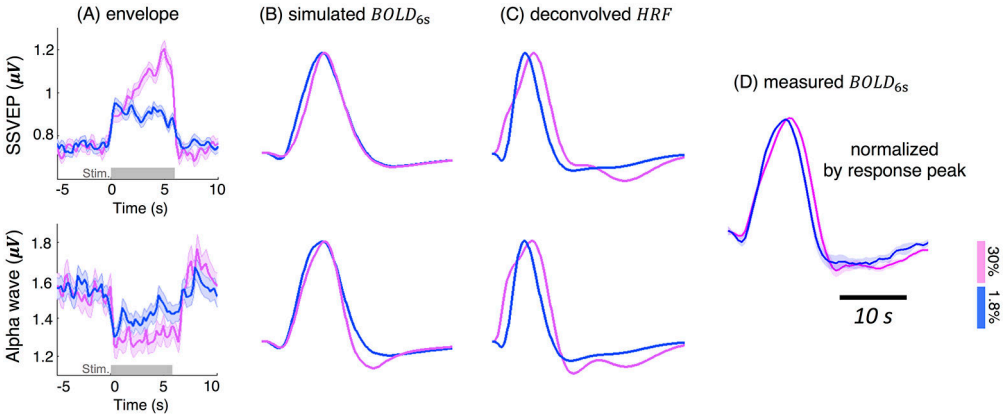

Figure 3.

Contrast-dependent patterns of SSVEP/alpha oscillations (A, mean and standard errors across all 6-s trials and all subjects) and the predicted BOLD responses (B, C); all BOLD responses were normalized by the peak intensity for comparisons. 'simulated $BOLD_{6s}$': simulated hemodynamic changes elicited by the 6-s stimuli, according to the EEG-based forward biophysical modeling (*Model I* 'Balloon Model'); 'deconvolved *HRF*': $HRF_{1.8\%}$ and $HRF_{30\%}$ derived by linearly deconvolving EEG signatures from fMRI measurements (*Model II* 'Deconvolution Model'); 'measured $BOLD_{6s}$': fMRI responses evoked by the 6-s stimuli, normalized by response peaks (Fig. 1B).

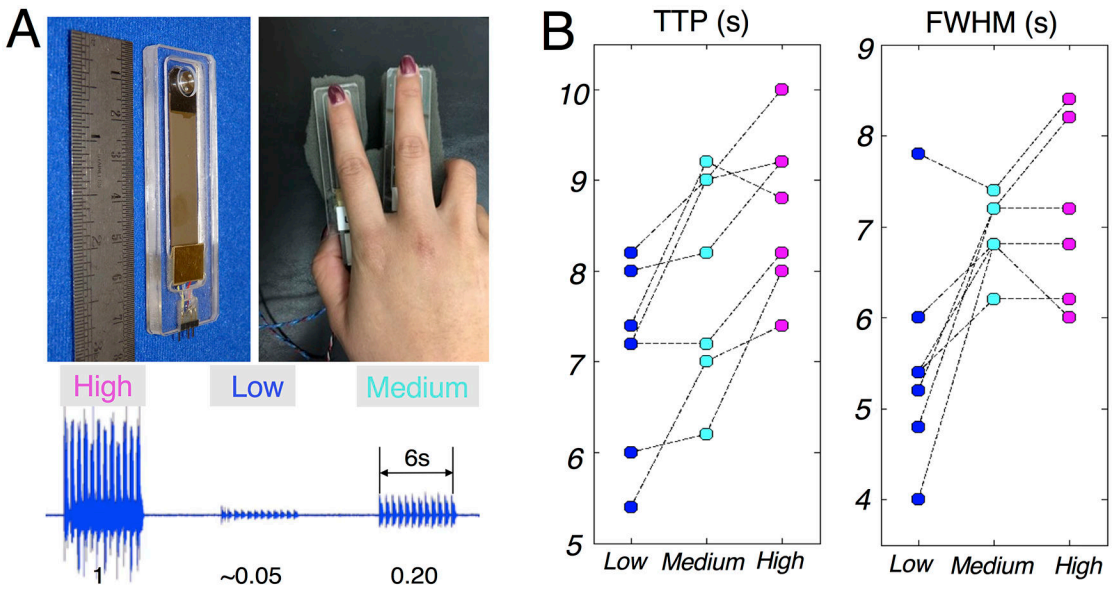

Figure 4.

(A) Illustration of the vibrotactile stimulator and hand position (top); mechanical vibration produced by the stimulators at different contrast levels (0.05/0.20/1), quantified by an accelerometer attached to the vibrotactile stimulator (bottom). (B) Summary of TTPs and FWHMs of fMRI responses evoked by different task contrasts (each dashed line connects the results from the same subject).

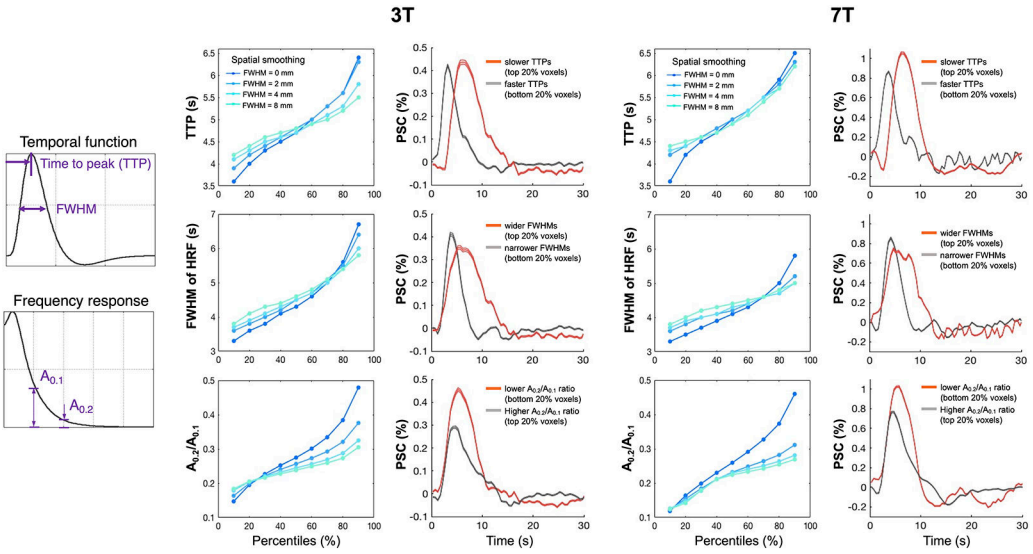

Figure 5.

Demonstration of remarkable inter-voxel HRF variability and the influence of voxel size (manipulated through spatial smoothing) on the heterogeneity of various HRF features. For each field strength, results from all task-active voxels (F-score > 15) and subjects were combined for display: (left column) percentile values of various features quantifying the HRF speed; (right column) HRFs sorted according to the percentiles of different temporal features (mean and standard errors across all voxels, 'PSC': percent signal change). Increased variability at high-resolutions was consistently observed when we varied the F-score threshold from 10 to 20.

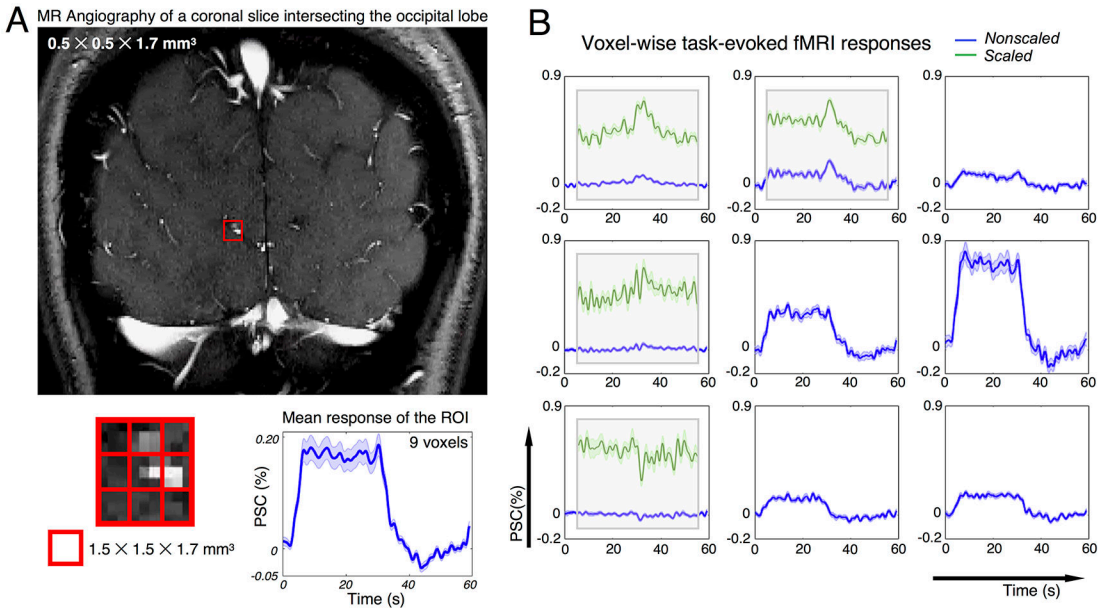

Figure 6.

HRFs depend on local vascular anatomy; and smaller voxel size can resolve spatially-varying HRF patterns that deviate from canonical hemodynamic models. (A) MR angiography of a coronal slice intersecting the calcarine sulcus (top); task-evoked fMRI signals averaged across 9 voxels in the red grid (mean and standard errors across all task trials, bottom). (B) Percent signal changes (PSCs) of task-evoked BOLD fMRI responses within each voxel shown in the red grid (mean and standard error across all trials). fMRI responses with modest percent signal change were scaled and displayed atop the original time course for better visualization (green curve, '*Scaled*'). Acquisition and experimental details of this dataset are described in Supplementary Material SM5.

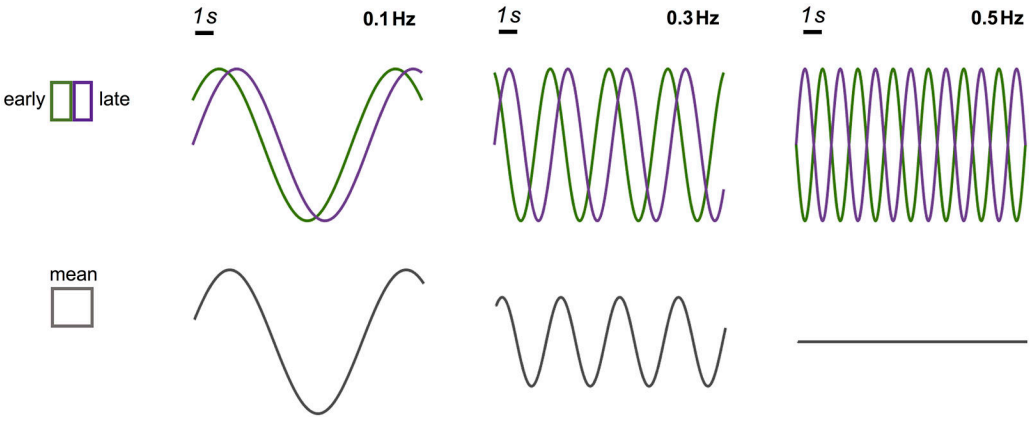

Figure 7.

Demonstration of how frequency-dependent signal reduction could arise from intra-voxel phase cancellation. In this simulation, while the early and late fMRI oscillations have identical amplitudes across frequencies, a 1 s temporal lag will lead to varying levels of intra-voxel dephasing (phase cancellation between early and late fMRI responses), and thereby signal reduction, at different oscillating frequencies. Therefore, smaller voxels (which discern early and late responses) can mitigate intra-voxel phase cancellation, enhancing the sensitivity to higher-frequency oscillations.